Upconversion Nano-Bioprobe

DOI: 10.1002/ange.201309503

Lanthanide-Doped $LiLuF_4$ Upconversion Nanoprobes for the Detection of Disease Biomarkers**

*Ping Huang, Wei Zheng, Shanyong Zhou, Datao Tu, Zhuo Chen, Haomiao Zhu, Renfu Li, En Ma, Mingdong Huang, and Xueyuan Chen**

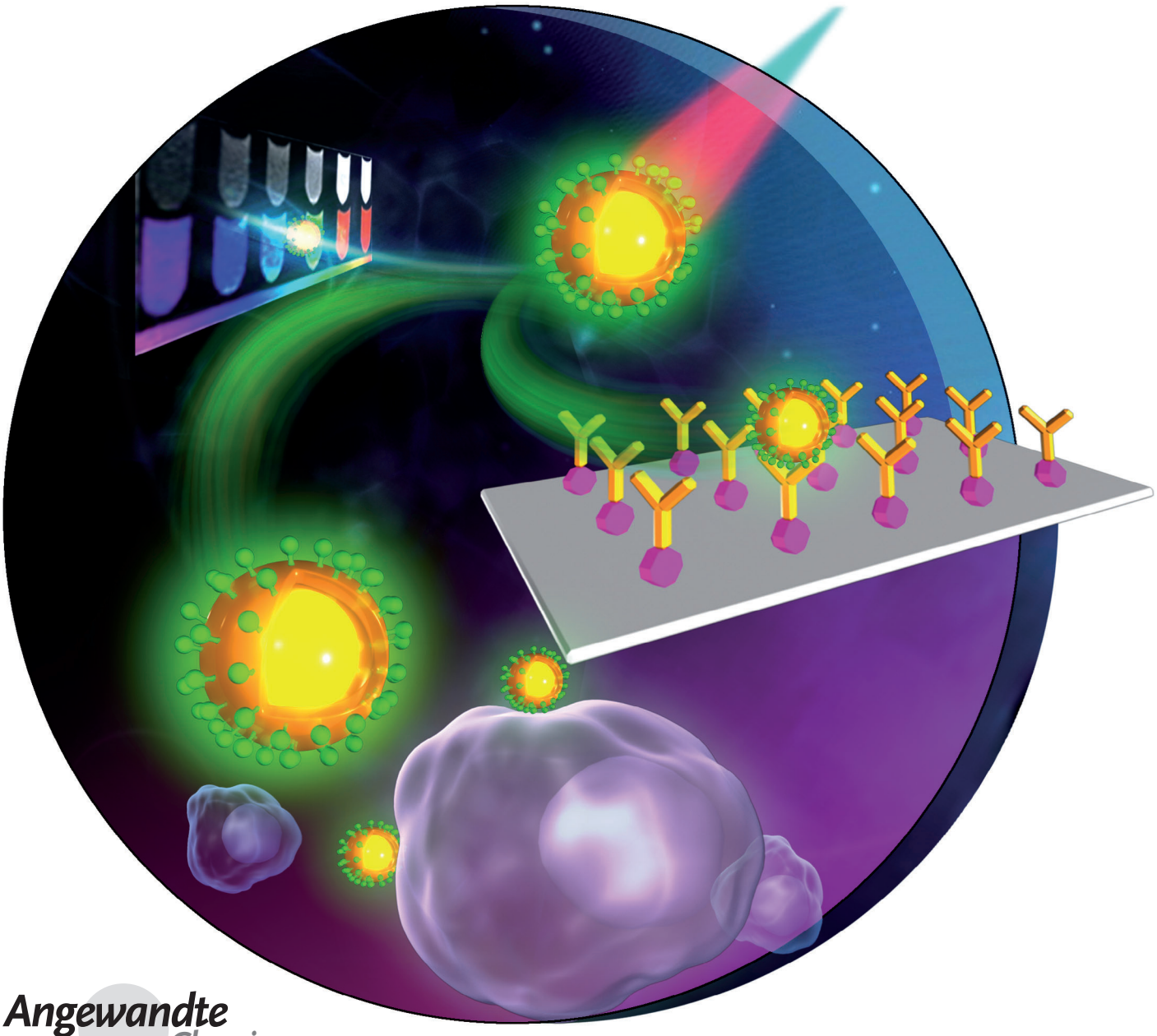

Abstract: *Lanthanide-doped upconversion nanoparticles (UCNPs) have shown great promise in bioapplications. Exploring new host materials to realize efficient upconversion luminescence (UCL) output is a goal of general concern. Herein, we develop a unique strategy for the synthesis of novel $LiLuF_4$:Ln^{3+} core/shell UCNPs with typically high absolute upconversion quantum yields of 5.0 % and 7.6 % for Er^{3+} and Tm^{3+}, respectively. Based on our customized UCL biodetection system, we demonstrate for the first time the application of $LiLuF_4$:Ln^{3+} core/shell UCNPs as sensitive UCL bioprobes for the detection of an important disease marker β subunit of human chorionic gonadotropin (β-hCG) with a detection limit of 3.8 ng mL^{-1}, which is comparable to the β-hCG level in the serum of normal humans. Furthermore, we use these UCNPs in proof-of-concept computed tomography imaging and UCL imaging of cancer cells, thus revealing the great potential of $LiLuF_4$:Ln^{3+} UCNPs as efficient nano-bioprobes in disease diagnosis.*

Lanthanide-doped upconversion nanoparticles (UCNPs) have evoked considerable interest owing to their superior features, such as high photochemical stability, large anti-Stokes shifts, long photoluminescence (PL) lifetimes, and low toxicity, which make them extremely suitable for use as alternatives to conventional downshifting luminescent bioprobes such as organic fluorescent dyes or quantum dots for various bioapplications.[1] Along with the remarkable light penetration depth and the absence of autofluorescence in biological specimens under near-infrared (NIR) excitation, these UCNPs are ideal for use as luminescent nanoprobes in biodetection and bioimaging.[2] Currently, the major bottleneck of UCNPs lies in their low upconversion (UC) quantum yield (QY), which is primarily ascribed to the intrinsic limitation of the host matrices and the surface quenching effect in colloidal dispersions. To make up for these deficiencies, growing a uniform shell with similar lattice constants is considered to be an effective way to improve the UC luminescence (UCL) efficiency of UCNPs.[3] Therefore, it is fundamentally important to develop a general approach for the synthesis of high-quality core/shell UCNPs and explore new host materials for lanthanide (Ln^{3+}) doping, in order to achieve high UCL output and promote their applications in biodetection and bioimaging.

Among diverse Ln^{3+}-doped inorganic nanoparticles (NPs), fluoride crystals are known to possess a host lattice of low phonon energies ($< 350\ cm^{-1}$), which results in decreased nonradiative relaxation and, in turn, yields a relatively high UCL efficiency.[4] The controlled synthesis, optical properties, and bioapplications of $LiLuF_4$, which is a potentially efficient host material for UCL, to the best of our knowledge has not been reported before. Herein, we reveal a strategy based on the successive layer-by-layer (LBL) injection of shell precursors for the synthesis of $LiLuF_4$:Ln^{3+} (Ln = Yb, Er, Tm) core/shell UCNPs through a thermal decomposition route. The resulting core/shell UCNPs yield enhanced UCL. To quantitatively evaluate the UCL efficiency, we measured their absolute UC QY. By utilizing the superior UCL of these $LiLuF_4$:Ln^{3+} core/shell UCNPs, we demonstrate the sensitive detection of an important pregnancy and tumor marker, β subunit of human chorionic gonadotropin (β-hCG), in a heterogeneous UCL bioassay. We also show the use of these nanoprobes in computed tomography (CT)/UCL dual-mode bioimaging in proof-of-concept experiments.

The $LiLuF_4$ crystal has a tetragonal structure (space group $I4_1/a$) with single site symmetry of S_4 for all Lu^{3+} ions.[5] High-quality $LiLuF_4$:Ln^{3+} core-only and core/shell UCNPs were synthesized by a thermal decomposition method (Figure 1 a). The as-synthesized NPs were hydrophobic and can be readily dispersed in a variety of nonpolar organic solvents, such as cyclohexane, forming a transparent colloidal solution. Transmission electron microscope (TEM) image shows that the as-synthesized $LiLuF_4$:Yb,Er core-only NPs were roughly rhomboid, with an average length of 28 ± 1.5 nm (Figure 1 b). Compositional analysis by energy-dispersive X-ray spectroscopy revealed the existence of Lu, F, and doped Yb ions in $LiLuF_4$:Yb,Er (20/1 %) core-only NPs (Supporting Information, Figure S1). In addition to the core-only NPs, core/shell NPs with tunable shell thickness were also obtained through epitaxial growth of inert $LiLuF_4$ shells on the core NPs through the successive LBL injection of shell precursors (Figure 1 a; see also the Experimental Section in the Supporting Information). TEM images show an increase in particle size for $LiLuF_4$:Yb,Er@$LiLuF_4$ core/shell NPs obtained by coating with 8- and 16-monolayer (ML) $LiLuF_4$ shells, respectively (Figure 1 c,d). Upon successive shell growth, the size of the core/shell NPs increased gradually from 28 ± 1.5 nm (core-only) to 39.8 ± 2.5 nm (8 ML) and 50.7 ± 2.8 nm (16 ML), which are in line with their narrower XRD peaks (Figure S2). The morphologies of the core-only and core/shell NPs were different from each other, owing to anisotropic shell growth.[3d] The corresponding high-resolution TEM (HRTEM) images exhibit clear lattice fringes with

[*] P. Huang, Dr. W. Zheng, Dr. D. T. Tu, Dr. H. M. Zhu, R. F. Li, E. Ma, Prof. X. Y. Chen
Key Laboratory of Optoelectronic Materials Chemistry and Physics, and Key Laboratory of design and assembly of functional nanostructures, Fujian Institute of Research on the Structure of Matter, Chinese Academy of Sciences, Fuzhou, Fujian 350002 (China)
E-mail: xchen@fjirsm.ac.cn
S. Y. Zhou, Dr. Z. Chen, Prof. M. D. Huang
State Key Laboratory of Structural Chemistry and Danish-Chinese Centre for Proteases and Cancer, Fujian Institute of Research on the Structure of Matter, Chinese Academy of Sciences
Fuzhou, Fujian 350002 (China)
P. Huang
University of Chinese Academy of Sciences, Beijing 100049 (China)

[**] We thank Prof. Fuyou Li and Dr. Wei Feng for the computed tomography experiments and cellular imaging. This work was supported by the 863 and 973 programs of MOST (2011AA03A407 and 2014CB845605), Special Project of National Major Scientific Equipment Development of China (2012YQ120060), the NSFC (11104266, 11204302, 11304314, 51002151, U1305244, and 21325104), Strategic Priority Research Program and Scientific Equipment Development Project of CAS (XDA09030307 and YZ201210).

Supporting information for this article, including detailed experimental procedures, is available on the WWW under http://dx.doi.org/10.1002/anie.201309503.

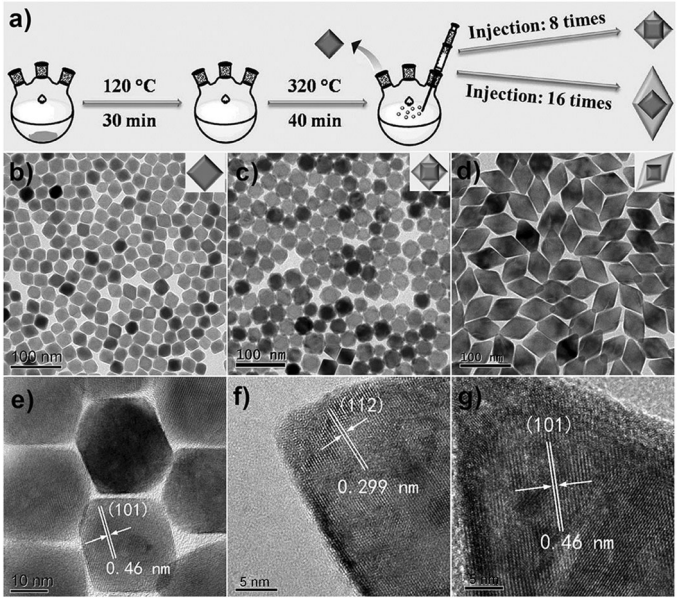

Figure 1. a) Synthesis of $LiLuF_4$:Ln^{3+} core-only and core/shell UCNPs. b–d) TEM images of $LiLuF_4$:Yb,Er core-only (b) and core/shell UCNPs with 8 MLs (c) and 16 MLs (d). e–g) The corresponding HRTEM images for (b–d).

observed d spacing of 0.46 nm for the (101) plane and 0.30 nm for the (112) plane of tetragonal-phase $LiLuF_4$ (JCPDS No. 027-1251), thus verifying the high crystallinity of the UCNPs (Figure 1 e–g). Compared to the LBL method recently developed by Zhang and co-workers,[6] our strategy is much easier to handle without the need for the precipitation of core NPs and the tedious alterative injection of different shell precursors, thus providing a more convenient and general synthetic method for core/shell UCNPs. More importantly, due to the successive surface passivation, homogeneous shells on the active core NPs can be expected, which was found to effectively protect the UCNPs from surface quenching, as will be demonstrated below.

Under 980 nm NIR laser irradiation, the colloidal cyclohexane solution of the resulting UCNPs displayed intense green (for Yb/Er co-doped UCNPs) or blue (for Yb/Tm co-doped UCNPs) UCL, which became brighter with increasing the shell layers (Insets of Figure 2 a,b). UCL spectra show that all NPs exhibited sharp and characteristic emission peaks, which can be exclusively attributed to the intra-4f electronic transitions of Er^{3+} and Tm^{3+}. Upon increasing the shell layers, the UCL intensity and lifetime of both Er^{3+} and Tm^{3+} were found to increase markedly (Figure 2 a,b; see also Figures S3 and S4, and Table S1). For example, the overall UCL intensity was remarkably enhanced by a factor of about 5.6 and 14.4 in $LiLuF_4$:Yb,Er core/shell UCNPs with 8 and 16 MLs, respectively, in comparison with their core-only counterparts; the corresponding UCL lifetime of $^4S_{3/2}$ of Er^{3+} increased from 0.14 ms to 0.60 and 0.87 ms, respectively. Both enhanced UCL intensity and lengthened lifetime in core/shell UCNPs solidly confirm the epitaxial surface passivation and the increased isolation of the core from its environment.[3b,7] The absolute UC QY, defined as the ratio of the number of emitted photons to the number of absorbed photons, was determined to be 0.11 % for Yb/Er co-doped core-only UCNPs, and 3.6 % and 5.0 % for Yb/Er co-doped core/shell UCNPs with 8 and 16 MLs, respectively, upon 980 nm NIR laser excitation at a power density of 127 $W cm^{-2}$. Similarly, the absolute UC QY was determined to be 0.61 %, 6.7 %, and 7.6 % for their Yb/Tm co-doped counterparts. It should be noted that the UC QYs for Yb/Er (or Yb/Tm) co-doped core/shell UCNPs with 16 MLs are the highest, as compared to those for Ln^{3+}-doped fluoride UCNPs, ever reported upon NIR excitation at equivalent power density (Table S2).[4a,8] Such high UC QYs achieved in $LiLuF_4$:Ln^{3+} core/shell UCNPs clearly demonstrate that the $LiLuF_4$ crystal is a promising host material for UCL, and are indicative of its potential use as sensitive UCL bioprobes for versatile bioapplications.

To render the as-prepared UCNPs hydrophilic and biocompatible, we removed the oleate ligands from their surface by acid treatment.[9] The successful removal of surface ligands was confirmed by Fourier transform infrared (FTIR) spectra and thermogravimetric analysis (TGA) of the NPs before and after acid treatment (Figures S5 and S6). As a result, these ligand-free UCNPs showed much better water solubility and can be steadily dispersed in distilled water for months, even at a high concentration of up to 80 $mg mL^{-1}$, without any observable aggregation (Figure S7). Such acid treatment had no noticeable influence on the size and morphology of UCNPs (Figures S7 and S8). Due to the deposition of uniform shells, derived from successive injection of shell precursors, on the core NPs, the ligand-free core/shell UCNPs with 16 MLs preserved the

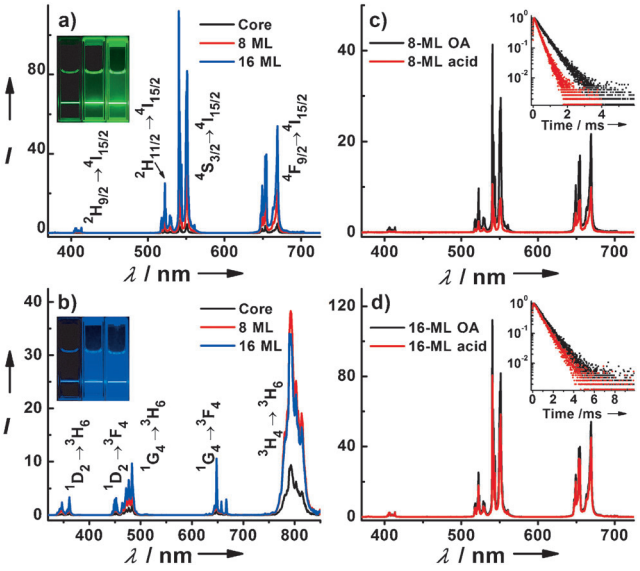

Figure 2. UCL spectra of a) $LiLuF_4$: 20 % Yb^{3+}, 1 % Er^{3+} and b) $LiLuF_4$: 20 % Yb^{3+}, 0.5 % Tm^{3+} core-only and core/shell UCNPs with different shell layers upon NIR excitation at 980 nm. The insets show the corresponding UCL photographs under 980 nm NIR laser irradiation at a power density of 20 $W cm^{-2}$. c,d) UCL spectra for oleate-capped and ligand-free $LiLuF_4$:Yb,Er core/shell UCNPs with 8 MLs (c) and 16 MLs (d). The insets show the corresponding UCL decays from $^4S_{3/2}$ by monitoring the Er^{3+} emission at 540.5 nm.

intense UCL of their parent NPs with a nearly unaltered UCL lifetime; this was remarkably different from those with 8 MLs, where the UCL intensity and lifetime were found to decrease significantly (Figure 2c,d; see also Figures S9–S11). In addition, due to the removal of surface ligands, positively charged Ln^{3+} ions were exposed on the surface of the ligand-free UCNPs, leaving their colloidal solution a positive ζ potential of +26.1 mV at pH 6.5 (Figure S12). As a consequence, these ligand-free UCNPs are enabled for direct conjugation in water with electronegative groups of hydrophilic and biocompatible molecules for various bioapplications.[9,10]

By utilizing their superior UCL, we explored these ligand-free UCNPs for heterogeneous UC-based biodetection after conjugation with avidin. Thanks to the bare Ln^{3+} ions on the surface of the ligand-free UCNPs, the electronegative groups of avidin can be conjugated to the surface of UCNPs through electrostatic attraction. The appearance of amide bands in the FTIR spectrum, and the differences in decomposition temperature, weight loss, and ξ potential for NPs before and after surface modification, revealed the successful conjugation of avidin to the surface of the UCNPs (Figures S5, S6, and S12). Consequently, these avidin-functionalized UCNPs could capture the biotinylated biomolecules through the strong avidin–biotin interaction.[11] By virtue of the high specific recognition of the captured molecules with the analytes, these avidin-functionalized UCNPs can be used as UC-based bioprobes for the detection of disease biomarkers in a heterogeneous bioassay.[12] By utilizing our customized UCL biodetection system combined with a microplate reader, we employed these avidin-functionalized UCNPs as UCL bioprobes for the detection of trace amounts of β-hCG through specific antibody–antigen recognition, where the β-hCG antigen was selected as analyte and the biotinylated β-hCG antibody was used to target the analyte for UCNP labeling. The UCL bioassay of β-hCG is illustrated in Figure 3a, and β-hCG was quantified by measuring the integrated UCL intensity of the UCNPs that were conjugated to the biotinylated β-hCG antibody (which was itself bound to β-hCG antigen). The observed UCL signal gradually increased along with the amount of β-hCG antigen bound to the well (Figure 3b). For comparison, we conducted a nonbinding control experiment by replacing the β-hCG antigen with bovine serum albumin (BSA) under otherwise identical conditions. Because there is no specific binding between BSA and the biotinylated β-hCG antibody, the UCL signal was hardly detectable (Figure S13). The calibration curve for UCL detection of the β-hCG antigen exhibits a nearly linear dependence at 0–310 ng mL^{-1}, and tends to saturate when the concentration exceeds 600 ng mL^{-1} (Figure 3c). The limit of detection (LOD), defined as the concentration that corresponds to three times the standard deviation above the signal measured in the control experiment, is approximately 3.8 ng mL^{-1}, which is comparable to the β-hCG level in the serum of normal humans.[13] These results reveal the great potential of the avidin-functionalized $LiLuF_4$:Ln^{3+} UCNPs as a sensitive UC-based bioprobe for the detection of disease markers.

Considering the high X-ray absorption capability of lutetium from the matrix, and the intense UCL from the

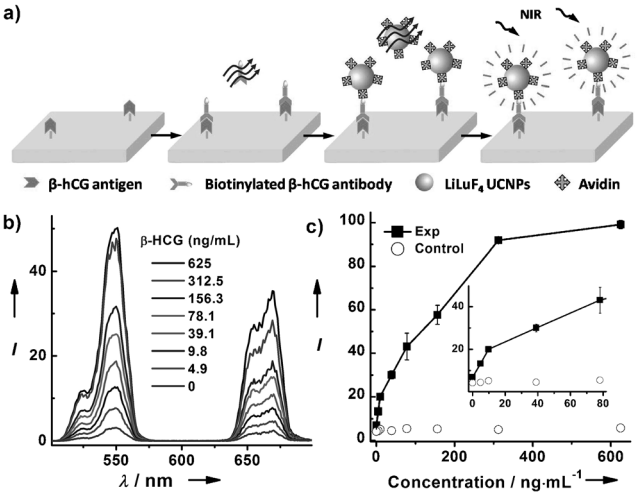

Figure 3. a) The process and principle of heterogeneous UCL detection of β-hCG. b) UCL spectra of the bioassays using $LiLuF_4$:Yb,Er@$LiLuF_4$ core/shell UCNPs with 16 MLs as a function of β-hCG concentration, each data point represents an average of three measurements. c) Calibration curve of UCL detection for the integrated UCL intensity versus the concentration of β-hCG. The control experiment was conducted using BSA instead of the β-hCG antigen as analyte under otherwise identical conditions.

doped Ln^{3+} emitters, these $LiLuF_4$:Ln^{3+} UCNPs may be used in CT/UCL dual-mode bioimaging. As a proof-of-concept experiment, we recorded in vitro phantom and color-mapped CT images using an aqueous solution of ligand-free UCNPs in concentrations of 0–39 mg mL^{-1}. As the concentration of UCNPs increased, the CT positive contrast enhancement signals increased in both phantom and color-mapped CT images (Figure 4a,b). To quantitatively evaluate the X-ray attenuation capability of these UCNPs, we measured the CT value, expressed in Hounsfield units (HU), of the UCNPs at different concentrations. As shown in Figure 4c, the CT value of the UCNPs at a concentration of 10 mg mL^{-1} is 149.4 HU, which is higher than that of the commercial CT contrast agent, iopromide (135.4 HU at the same concentration).[14] These results indicate that $LiLuF_4$ UCNPs show great promise as efficient CT contrast agents.

Furthermore, we employed $LiLuF_4$:Ln^{3+} UCNPs for targeted cellular imaging after coupling with the amino-terminal fragment (ATF) of urokinase plasminogen activator (uPA, an important marker of tumor biology and metastasis).[15] Human lung cancer cells (H1299) with uPA receptors (uPARs) overexpressed on the membrane were selected as the target cancer cells, and the specific recognition capability of ATF-coupled UCNPs was examined by means of confocal laser scanning microscopy (CLSM). Owing to the high binding affinity between ATF and uPAR ($K_d \approx 0.28$ nM),[16] ATF-coupled $LiLuF_4$:Yb,Er UCNPs can be specifically targeted to H1299 cells after coincubation in a culture medium at 37 °C for 2 h. As a result, intense green and red UCL signals of Er^{3+} were observed surrounding H1299 cells upon 980 nm NIR laser excitation (Figure 4d). For comparison, we also conducted control experiments using human embryo lung fibroblast (HELF) cells, in which the

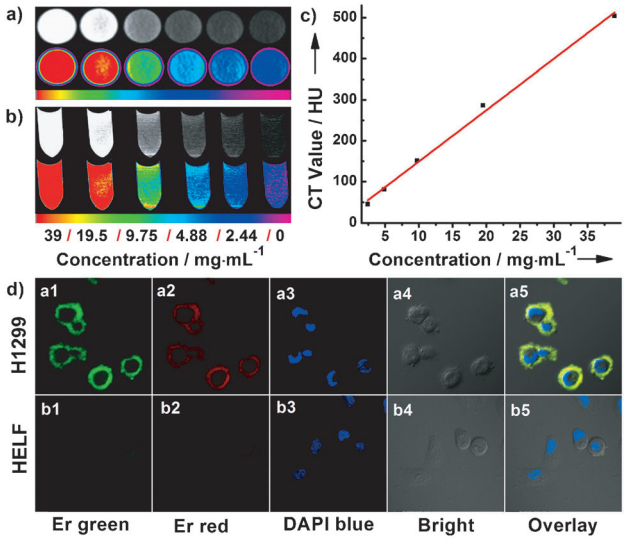

Figure 4. The phantom and color-mapped CT images of the a) cross section and b) longitudinal section of the centrifuge tubes. c) The CT value (HU) of aqueous solution of the ligand-free $LiLuF_4$:Yb,Er@$LiLuF_4$ core/shell UCNPs with 16 MLs at different concentrations. d) CLSM images of (a1–a5) H1299 and (b1–b5) HELF cells after incubation with ATF-coupled $LiLuF_4$:Yb,Er@$LiLuF_4$ core/shell UCNPs with 16 MLs. Panels 1–4 show the green UCL, red UCL, DAPI blue image, and bright-field image, respectively. Panel 5 is the overlay image of panels 1–4.

expression of uPAR is low, under identical imaging conditions. The green and red signals of Er^{3+} were hardly observed on the surface of HELF cells, owing to the lack of specific recognition between ATF-coupled UCNPs and HELF cells. Likewise, when employing ATF-coupled $LiLuF_4$:Yb,Tm UCNPs as probes for targeted UCL imaging, we observed intense blue and red UCL of Tm^{3+} on H1299 cells (Figure S14). The dark cytotoxicity and phototoxicity of ATF-coupled UCNPs were measured on HELF cells using a cell counting kit (CCK-8) assay. The cell viability was determined to be greater than 90%, even at a high concentration of 1 mg mL^{-1} for ATF-coupled UCNPs, either in the dark or upon 980 nm NIR light irradiation, for 2 min (Figure S15). The high cell viability implies that ATF-coupled $LiLuF_4$:Ln^{3+} UCNPs are biocompatible and virtually nontoxic to live cells. These results clearly demonstrate that $LiLuF_4$:Ln^{3+} UCNPs coupled with specific capture molecules for tumor markers can be used as bioprobes in targeted UCL imaging of cancer cells.

In summary, we have developed a facile strategy based on successive LBL injection of shell precursors for the synthesis of $LiLuF_4$:Ln^{3+} core/shell UCNPs. Due to the valid surface passivation, the UCNPs yielded improved UCL, and the absolute UC QY was significantly enhanced, with a record-high value of 5.0% for Er^{3+} and 7.6% for Tm^{3+} in core/shell UCNPs with 16 MLs. By means of our customized UCL biodetection system, we employed the avidin-functionalized $LiLuF_4$:Yb,Er core/shell UCNPs as sensitive UCL bioprobes for the detection of β-hCG, a disease biomarker with a detection limit down to 3.8 ng mL^{-1}, which is comparable to the β-hCG level in the serum of normal humans. Furthermore, we revealed the great potential of these UCNPs as multimodal nanoprobes in CT/UCL bioimaging. These findings may open up new avenues for the exploration of $LiLuF_4$:Ln^{3+} UCNPs in versatile bioapplications. The facile synthetic strategy we propose can be easily extended to the synthesis of other highly efficient UCL nano-bioprobes.

Received: November 1, 2013

Keywords: biodetection · disease biomarkers · nanoprobes · $LiLuF_4$ · upconversion

[1] a) J. Wang, P. A. Tanner, *J. Am. Chem. Soc.* **2010**, *132*, 947–949; b) A. Gnach, A. Bednarkiewicz, *Nano Today* **2012**, *7*, 532–563; c) J. C. G. Bünzli, S. V. Eliseeva, *Chem. Sci.* **2013**, *4*, 1939–1949; d) H. H. Gorris, O. S. Wolfbeis, *Angew. Chem.* **2013**, *125*, 3668–3686; *Angew. Chem. Int. Ed.* **2013**, *52*, 3584–3600; e) Y. X. Liu, D. S. Wang, J. X. Shi, Q. Peng, Y. D. Li, *Angew. Chem.* **2013**, *125*, 4462–4465; *Angew. Chem. Int. Ed.* **2013**, *52*, 4366–4369; f) J. Zhao, D. Jin, E. P. Schartner, Y. Lu, Y. Liu, A. V. Zvyagin, L. Zhang, J. M. Dawes, P. Xi, J. A. Piper, E. M. Goldys, T. M. Monro, *Nat. Nanotechnol.* **2013**, *8*, 729–734; g) D. E. Achatz, R. J. Meier, L. H. Fischer, O. S. Wolfbeis, *Angew. Chem.* **2011**, *123*, 274–277; *Angew. Chem. Int. Ed.* **2011**, *50*, 260–263.

[2] a) G. Y. Chen, J. Shen, T. Y. Ohulchanskyy, N. J. Patel, A. Kutikov, Z. P. Li, J. Song, R. K. Pandey, H. Agren, P. N. Prasad, G. Han, *ACS Nano* **2012**, *6*, 8280–8287; b) Y. Park, H. M. Kim, J. H. Kim, K. C. Moon, B. Yoo, K. T. Lee, N. Lee, Y. Choi, W. Park, D. Ling, K. Na, W. K. Moon, S. H. Choi, H. S. Park, S. Y. Yoon, Y. D. Suh, S. H. Lee, T. Hyeon, *Adv. Mater.* **2012**, *24*, 5755–5761; c) W. Fan, B. Shen, W. Bu, F. Chen, K. Zhao, S. Zhang, L. Zhou, W. Peng, Q. Xiao, H. Xing, J. Liu, D. Ni, Q. He, J. Shi, *J. Am. Chem. Soc.* **2013**, *135*, 6494–6503; d) P. A. Ma, H. H. Xiao, X. X. Li, C. X. Li, Y. L. Dai, Z. Y. Cheng, X. B. Jing, J. Lin, *Adv. Mater.* **2013**, *25*, 4898–4905; e) Y. H. Wang, H. G. Wang, D. P. Liu, S. Y. Song, X. Wang, H. J. Zhang, *Biomaterials* **2013**, *34*, 7715–7724.

[3] a) N. J. J. Johnson, A. Korinek, C. H. Dong, F. C. J. M. van Veggel, *J. Am. Chem. Soc.* **2012**, *134*, 11068–11071; b) F. Zhang, R. C. Che, X. M. Li, C. Yao, J. P. Yang, D. K. Shen, P. Hu, W. Li, D. Y. Zhao, *Nano Lett.* **2012**, *12*, 2852–2858; c) H. Schäfer, P. Ptacek, K. Hickmann, M. Prinz, M. Neumann, M. Haase, *Russ. J. Inorg. Chem.* **2009**, *54*, 1914–1920; d) C. Zhang, J. Y. Lee, *ACS Nano* **2013**, *7*, 4393–4402.

[4] a) G. Y. Chen, T. Y. Ohulchanskyy, A. Kachynski, H. Agren, P. N. Prasad, *ACS Nano* **2011**, *5*, 4981–4986; b) M. Haase, H. Schafer, *Angew. Chem.* **2011**, *123*, 5928–5950; *Angew. Chem. Int. Ed.* **2011**, *50*, 5808–5829; c) Y. F. Wang, G. Y. Liu, L. D. Sun, J. W. Xiao, J. C. Zhou, C. H. Yan, *ACS Nano* **2013**, *7*, 7200–7206.

[5] G. D. Brunton, H. Insley, T. N. McVay, R. E. Thoma, *Oak Ridge Natl. Lab. Rep.* **1965**, *3761*, 52.

[6] X. M. Li, D. K. Shen, J. P. Yang, C. Yao, R. C. Che, F. Zhang, D. Y. Zhao, *Chem. Mater.* **2013**, *25*, 106–112.

[7] F. Wang, J. A. Wang, X. G. Liu, *Angew. Chem.* **2010**, *122*, 7618–7622; *Angew. Chem. Int. Ed.* **2010**, *49*, 7456–7460.

[8] a) J. C. Boyer, F. van Veggel, *Nanoscale* **2010**, *2*, 1417–1419; b) C. T. Xu, P. Svenmarker, H. C. Liu, X. Wu, M. E. Messing, L. R. Wallenberg, S. Andersson-Engels, *ACS Nano* **2012**, *6*, 4788–4795; c) H. C. Liu, C. T. Xu, D. Lindgren, H. Y. Xie, D. Thomas, C. Gundlach, S. Andersson-Engels, *Nanoscale* **2013**, *5*, 4770–4775.

[9] G. A. Ozin, N. Bogdan, F. Vetrone, J. A. Capobianco, *Nano Lett.* **2011**, *11*, 835–840.

[10] Y. Zhang, F. Zheng, T. Yang, W. Zhou, Y. Liu, N. Man, L. Zhang, N. Jin, Q. Dou, Y. Zhang, Z. Li, L. P. Wen, *Nat. Mater.* **2012**, *11*, 817 – 826.
[11] X. Zeng, Y. X. Sun, W. Qu, X. Z. Zhang, R. X. Zhuo, *Biomaterials* **2010**, *31*, 4771 – 4780.
[12] J. C. G. Bünzli, *Chem. Rev.* **2010**, *110*, 2729 – 2755.
[13] F. T. I. Marcillac, J-M. Bidart, P. Ghillani, V. Ribrag, *Cancer Res.* **1992**, *52*, 3901 – 3907.
[14] X. J. Zhu, J. Zhou, M. Chen, M. Shi, W. Feng, F. Y. Li, *Biomaterials* **2012**, *33*, 4618 – 4627.
[15] W. Zheng, S. Y. Zhou, Z. Chen, P. Hu, Y. S. Liu, D. T. Tu, H. M. Zhu, R. F. Li, M. D. Huang, X. Y. Chen, *Angew. Chem.* **2013**, *125*, 6803 – 6808; *Angew. Chem. Int. Ed.* **2013**, *52*, 6671 – 6676.
[16] R. J. Goodson, M. V. Doyle, S. E. Kaufman, S. Rosenberg, *Proc. Natl. Acad. Sci. USA* **1994**, *91*, 7129 – 7133.

